Distorted Hexagonal Phase Studied by Neutron Diffraction: Lipid Components Demixed in a Bent Monolayer

Lai Ding,[†] Thomas M. Weiss,[‡] Giovanna Fragneto,[§] Wenhan Liu,[†,||] Lin Yang,[⊥] and Huey W. Huang*,[†]

Department of Physics & Astronomy, Rice University, Houston, Texas 77251, European Synchrotron Radiation Facility, 6 rue Jules Horowitz, BP 220, F-38043 Grenoble Cedex 9, France, Institut Laue-Langevin, 6 rue Jules Horowitz, BP 156, 38042 Grenoble Cedex 9, France, and National Synchrotron Light Source, Brookhaven National Laboratory, Upton, New York 11973

Received August 25, 2004. In Final Form: October 7, 2004

The recent discovery of a distorted hexagonal phase in 1,2-dioleoyl-*sn*-glycero-3-phosphatidylethanolamine/1,2-dioleoyl-*sn*-glycero-3-phosphatidylcholine (DOPE/DOPC) mixtures raised the intriguing question as to whether lipid mixtures demix in a bent monolayer. We performed neutron diffraction on a mixture of headgroup deuterated DOPC-d_{13} and nondeuterated DOPE to study the lipid distribution in the distorted hexagonal phase. The 1:1 lipid mixture in full hydration and 25 °C was in a homogeneous lamellar phase. Upon dehydration the mixture transformed to a rhombohedral phase, then to a distorted inverted hexagonal phase, and finally to a regular inverted hexagonal phase. In the distorted hexagonal phase, the diffraction pattern showed a two-dimensional monoclinic lattice with two reciprocal vectors of equal length (1.5 nm^{-1}) forming an angle 53° between them. Diffraction intensities measured while varying the D_2O/H_2O ratio in the humidity was used to solve the phase problem. The neutron scattering length density distribution of the distorted hexagonal phase was constructed. The constant density contours are approximately elliptical. The difference in the eccentricities of the contours between the water and lipid distributions indicates that the DOPE/DOPC ratio is not uniform around the elliptical lipid tube in the unit cell. DOPE is preferentially distributed at the vertex regions where the curvature is the highest. Thus for the first time it is shown that when a monolayer of a homogeneous lipid mixture is bent, the lipid components are partially demixed in reaching the free energy minimum.

Spontaneous curvature (SC) describes the minimum energy configuration of an unconstrained lipid monolayer.[1] The SC of each monolayer leaflet in a membrane can influence whether a structural change, such as fusion or pore formation, will occur. For example, a much discussed energy crisis for membrane fusion[2,3] was supposed to be caused by a high-energy barrier at the first intermediate state, but the barrier would not exist if the membrane leaflets have appropriate values of SC.[4,5] Empirical values of SC have been estimated from the radii of the circular lipid tubes formed in the inverted hexagonal phases.[6,7] Previous experiments also indicated that a homogeneous lipid mixture has a unique SC that is the linear combination of its component SCs.[7−9] However a distorted hexagonal phase of 1,2-dioleoyl-*sn*-glycero-3-phosphatidylethanolamine/1,2-dioleoyl-*sn*-glycero-3-phosphatidylcholine (DOPE/DOPC) mixtures was discovered recently. This raised the question[10] as to whether a lipid mixture has a unique SC under bending stress.

In this paper we report a neutron diffraction analysis of the distorted hexagonal phase formed by the 1:1 DOPC/DOPE mixture. To distinguish the two lipids, we used DOPC-d_{13} with its headgroup deuterated. The diffraction pattern exhibits a two-dimensional (2D) monoclinic lattice. The phases of the diffraction amplitudes were solved by the method of D_2O/H_2O exchange.[11] The constructed neutron scattering length density distribution shows that the lipids form elliptical tubes arranged in a two-dimensional array of distorted hexagons, hence designated as the $H_{II\delta}$ phase. From the scattering length density distributions of the water and the lipid in the $H_{II\delta}$ phase, we will show that DOPC and DOPE are not homogeneously mixed in the elliptical tube. The variation of the DOPE/DOPC ratio is consistent with the local curvature

* To whom correspondence may be addressed. Tel: 713 348-4899. Fax: 713 348-4150. E-mail: hwhuang@rice.edu.

[†] Rice University.

[‡] European Synchrotron Radiation Facility.

[§] Institut Laue-Langevin.

[||] On leave from Department of Physics, University of Sciences and Technology of China, Hefei, China.

[⊥] National Synchrotron Light Source.

(1) Helfrich, W. Elastic properties of lipid bilayers: theory and possible experiments. *Z. Naturforsch.* **1973**, *28c*, 693−703.

(2) Siegel, D. P. Energetics of intermediates in membrane fusion: comparison of stalk and inverted micellar intermediate mechanisms. *Biophys. J.* **1993**, *65*, 2124−2140.

(3) Siegel, D. P. The modified stalk mechanism of lamellar/inverted phase transitions and its implications for membrane fusion. *Biophys. J.* **1999**, *76*, 291−313.

(4) Kozlovsky, Y.; Kozlov, M. M. Stalk model of membrane fusion: solution of energy crisis. *Biophys. J.* **2002**, *82*, 882−895.

(5) Markin, V. S.; Albanesi, J. P. Membrane fusion: stalk model revisited. *Biophys. J.* **2002**, *82*, 693−712.

(6) Gruner, S. M.; Parsegian, V. A.; Rand, R. P. Directly measured deformation energy of phospholipid HII hexagonal phases. *Faraday Discuss. Chem. Soc.* **1986**, *81*, 29−37.

(7) Rand, R. P.; Fuller, N. L.; Gruner, S. M.; Parsegian, V. A. Membrane curvature, lipid segregation, and structural transitions for phospholipids under dual-solvent stress. *Biochemistry* **1990**, *29*, 76−87.

(8) Leikin, S.; Kozlov, M. M.; Fuller, N. L.; Rand, R. P.; Measured effects of diacylglycerol on structural and elastic properties of phospholipid membranes. *Biophys. J.* **1996**, *71*, 2623−2632.

(9) Chen, Z.; Rand, R. P. The influence of cholesterol on phospholipid membrane curvature and bending elasticity. *Biophys. J.* **1997**, *73*, 267−276.

(10) Yang, L.; Ding, L.; Huang, H. W. New Phases of Phospholipids and Implications to the membrane fusion problem. *Biochemistry* **2003**, *42*, 6631−6635.

(11) Ding, L.; Liu, W. H.; Wang, W. C.; Glinka, C. J.; Worcester, D. L.; Yang, L.; Huang, H. W. Diffraction techniques for nonlamellar phases of phospholipids. *Langmuir* **2004**, *20*, 9262−9269.

10.1021/la047876u CCC: $30.25
Published on Web 12/01/2004

around the elliptical tube. This should make us reexamine the free energy of bending for mixed-lipid membranes, for example, during membrane fusion[4,5] or pore formation.[12] This is important because cell membranes are normally made of lipid mixtures.

A distorted hexagonal phase has been found so far only in dehydrated conditions of lipids.[10] This is also true of the rhombohedral phase which contains the structure of the first intermediate state of fusion, i.e., the stalk.[13,14] We conjecture that the initial step of membrane fusion is necessarily the removal of water molecules between two contacting bilayers. Thus fusion must take place in a locally dehydrated condition. This makes the dehydration-induced rhombohedral phase and distorted hexagonal phase relevant to fusion occurring in physiological conditions. A recent theoretical investigation showed that the hydration (or dehydration) energy is the key to the stalk formation.[15]

Experimental Materials and Mehods

Materials. 1,2-Dioleoyl-*sn*-glycero-3-phosphatidylcholine with deuterated choline (DOPC-d_{13}) and 1,2-dioleoyl-*sn*-glycero-3-phosphatidylethanolamine (DOPE) were purchased from Avanti Polar Lipids (Alabaster, AL). Silicon wafers (⟨100⟩ surface, P-doped), 300 μm thick, were purchased from Virginia Semiconductor (Fredericksburg, VA). All materials were used as delivered.

Sample Preparation. Each silicon wafer was swabbed with Q-tips in ethanol first, then was sonicated several times in different solvents, each time for 5 min in chloroform, methanol, ethanol, or distilled water. At last the wafer was sonicated in ethanol and then dried in the oven.

Sample preparation followed the procedure described in Yang et al.[16] DOPC−DOPE mixtures were deposited from an organic solution on a cleaned silicon wafer. The organic solvent was a 3:1 trifluoroethanol (TFE)−chloroform mixture.[17] A 5 mg portion of lipid was spread over a 25 × 25 mm^2 wafer. The organic solvent was removed in a vacuum or evaporated in open air. The deposit was then hydrated with saturated water vapor at room temperature. Under this condition, the lipid spontaneously formed a stack of hydrated bilayers (in the L_α phase) parallel to the substrate.[10] The alignment was inspected by an X-ray two-dimensional $\omega-\theta$ scan.[18] A single lamellar pattern implied that the two lipid components were homogeneously mixed in this phase.

A U-shaped stand made of copper was used to support the wafers. The seat was 5 mm deep filled with spacers (made of copper), so the wafers could be inserted vertically and allowed a 20 × 25 mm^2 usable sample area. Six wafers were inserted into the stand. Thus our sample consisted of six parallel and separated silicon substrates, with 5 mg of lipid mixture coated on each. The separation between individual wafers was 0.5−1 mm, which in total made the sample about 5 mm thick. The lipid sample on each wafer was in direct contact with ambient air. Such neutron samples were first used by Yang et al.,[16] so the temperature and hydration of the sample could be changed rapidly (within minutes).

The sample was pre-examined by X-ray diffraction. At 25 °C, it showed four phases, i.e., the lamellar (L_α), rhombohedral (R), distorted hexagonal ($H_{II\delta}$), and regular hexagonal (H_{II}) as a function of the relative humidity (RH) of the ambient air. Above 80% RH, the DOPC-d_{13}/DOPE 1:1 mixture was in the L_α phase, from ∼80% to ∼60% RH in the R phase, from ∼60% to ∼52% RH in the $H_{II\delta}$ phase, and below ∼52% in the H_{II} phase. In most cases, the $H_{II\delta}$ phase coexisted either with a weak R phase or with a weak H_{II} phase. This RH dependence was reproduced by the neutron experiment on site, throughout the entire experimental period. This was an indication that there was no sample deterioration, since in an earlier experiment we noted a deteriorated lipid sample (as determined by thin-layer chromatography) changed its phase diagram. The phase diagram of DOPC-d_{13}/DOPE 1:1 mixture is similar to that of a nondeuterated DOPC/DOPE 1:1 mixture, shown in Yang et al.[10] As noted previously, the phase boundaries and the degree of coexistence were somewhat dependent on whether the sample was hydrating or dehydrating. Therefore it was impossible to determine if the deuteration of the DOPC headgroup had any effect on the details of the phase diagram. (In the case of diphytanoyl phosphatidylcholine, the deuteration of the headgroup significantly affected its phase diagram, Ding et al.[11]) As far as we could tell, hydration by D_2O (in place of H_2O) did not seem to affect the phase diagram.

Humidity Chamber. At the beamline D16 of the Institut Laue-Langevin, an aluminum chamber enclosed a goniometer head that held the sample and a separate water bath. The sample and water were separately heated; thus we were able to vary the relative humidity of the air immediately surrounding the sample. Two sensors, one for temperature and another for humidity, were positioned close to the sample to monitor the sample condition. The description of this humidity chamber was given previously by Perino-Gallice et al.[19]

Neutron Experiment. The method of diffraction from substrate-supported nonlamellar structures was described in detail by Yang and Huang.[14] The neutron experiment was performed at the beamline D16 of the Institut Laue-Langevin (ILL), Grenoble, France. Its instrumentation is described at the URL http://www.ill.fr/index_sc.html. Normally the beamline offers a vertically focused neutron beam by utilizing nine vertically bent polycrystalline graphite monochromators. For this experiment, we left the monochromators unfocused. But we noticed a substantial vertical divergence (see below). The neutron wavelength was 4.54 Å with a 1% spread, full width at half-maximum. The area detector (256 × 256 mm^2, 2 mm resolution) was seated on a radial arm of a circular track centered at the sample. The position of the detector on the radial arm was adjustable but limited by available vacuum beam paths. Our measurement was carried out with the detector−sample distance 767 mm. The complete diffraction pattern was recorded in three different geometries as described below. The experiment was conducted at temperature 25 °C and humidity 56% RH at five D_2O/H_2O ratios: 0:1, 1:3, 1:1, 3:1, 1:0.

1. Off-Specular Reflection with Vertical Substrates. Initially the sample substrates were oriented vertically with the plane of the substrate making a small angle with respect to the incident beam. A rectangular slit of 12 mm (height) × 8 mm (width) was used to define the incident neutron flux. The reflection showed a diffraction pattern with rectangularly shaped peaks (see Figure 1). The shape of the peaks is roughly the shape of the exposed sample. A specular reflection peak allowed us to determine the incident angle ω between the incident beam and the plane of the substrate. Also the attenuation of the scattering by the silicon wafers cast a line shadow on the detector in the direction of the plane of the wafers. This line shadow is exactly halfway between the beam center and the specular reflection peak.

The scan time was 5 h for D_2O/H_2O ratios 1/0 and 3/1 and 8 h for D_2O/H_2O ratios 1/1, 1/3, and 0/1.

2. Off-Specular Reflection with Horizontal Substrates. Next, neutron reflection was recorded with the sample substrates held horizontally (Figure 2). The beam slit was changed to 8 mm

(12) Zemel, A.; Fattal, D. R.; Ben-Shaul, A. Energetics and self-assembly of amphipathic peptide pores in lipid membranes. *Biophys. J.* **2003**, *84*, 2242−2255.
(13) Yang, L.; Huang, H. W. Observation of a membrane fusion intermediate structure. *Science* **2002**, *297*, 1877−1879.
(14) Yang, L.; Huang, H. W. A rhombohedral phase of lipid containing a membrane fusion intermediate structure. *Biophys. J.* **2003**, *84*, 1808−1817.
(15) Kozlovsky, Y.; Siegel, D. A.; Kozlov, M. M. Stalk phase formation: effects of dehydration and saddle splay modulus. *Biophys. J.* **2004**, *87*, 2508−2521.
(16) Yang, L.; Weiss, T. M.; Lehrer, R. I.; Huang, H. W. Crystallization of antimicrobial pores in membranes: magainin and protegrin. *Biophys. J.* **2000**, *79*, 2002−2009.
(17) Ludtke, S.; He, K.; Huang, H. W. Membrane thinning caused by magainin 2. *Biochemistry* **1995**, *34*, 16764−16769.
(18) Weiss, T. M.; van der Wel, P. C. A.; Killian, J. A.; Koeppe II, R. E.; Huang, H. W. Hydrophobic mismatch between helices and lipid bilayers. *Biophys. J.* **2003**, *84*, 379−385.
(19) Perino-Gallice, L.; Fragneto, G.; Mennicke, U.; Salditt, T.; Rieutord, F. Dewetting of solid supported multilamellar lipid layers. *Eur. Phys. J.* **2002**, *E8*, 275−282.

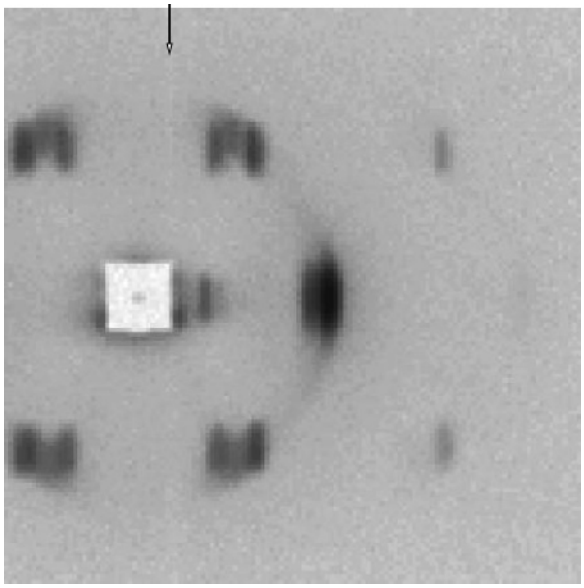

Figure 1. Reflection image produced by a vertical sample on the area detector. The sample substrates were vertical and 1.1° with respect to the incident beam. The hydration was by pure D_2O. The area detector (256 × 256 mm^2, 2 mm resolution) was movable on a circle of radius 767 mm centered at the sample. The central normal vector to the area detector was 4.98° from the incident beam, and the exposure time was 1 h. The beam center is visible through the beam stop. Along the right edge of the beam stop is the line shadow of the silicon wafers (indicated by an arrow). Twice the angle from the beam center to the line shadow is the specular reflection peak. The peaks are identified by referring to Figure 4 turned 90° clockwise with (0,0) as the beam center, so that q_z is horizontal. (0,1), (0,2), (−1,1) (1,0), and (1,1) are visible. The peak between (−1,1) and (1,0) and the peak on the left side of (0,1) belong to the coexisting regular hexagonal phase. The detector was also moved to 11° from the incident beam to detect possible higher orders in the high q_z region, e.g., (1,2). No higher order peaks were detected.

(height) × 12 mm (width). The line shadow of the silicon wafers showed that the substrates were not exactly horizontal. The reciprocal lattice of the diffraction pattern was based on this line shadow. The scan time was approximately 8 h for each of five D_2O/H_2O ratios. The peaks were smeared in the vertical direction due to the vertical beam divergence.

3. Oscillating ω Scan. The peaks along the reciprocal vector normal to the substrates were scanned by rotating the angle ω with the substrates oriented vertically. (Here we follow the convention of calling 2θ the angle between the incident beam and the diffraction beam, and ω is the angle between the incident and the plane of substrate.) Data were collected as ω was increased in steps $\Delta\omega = 0.125°$, 6 min per step for D_2O/H_2O ratio 1:0 (3 min for other D_2O/H_2O ratios), from $\omega = 0.25°$ to ∼10°. The complete data of the oscillating ω scan was the sum of the series of files, each collected at one ω-step (Figure 3).

Data Reduction. The data on the two-dimensional detector were first treated by the standard correction procedure for the instrumental background and detector sensitivity (see for example http://www.ill.fr/YellowBook/D11).

The diffraction patterns on the detector were transformed according to the diffraction geometries to the reciprocal space (q_x, q_z) where the z-axis is defined as normal to the plane of the substrates.[20] Two sets of lattice were found. One set of relatively weak peaks belongs to a regular hexagonal lattice with basis vector $\mathbf{b_1}(q_x = 0.145 \sin\gamma, q_z = 0.145 \cos\gamma)$ and $\mathbf{b_2}(0,0.145)$ at $\gamma = 60°$ in the unit of Å^{-1}. The majority of the peaks belong to a 2D monoclinic (space group $P2$, designated as the $H_{II\delta}$)) lattice (Figure 4). The reciprocal vectors for this lattice were $\mathbf{b_1}(q_x = 0.150 \sin\gamma, q_z = 0.150 \cos\gamma)$ and $\mathbf{b_2}(0,0.150)$ at $\gamma = 53°$. We ignored the weak coexisting phase. (The total integrated intensity of the coexisting hexagonal phase is less than a few percent of the total integrated intensity of the distorted hexagonal phase. Therefore the coexisting phase did not affect the analysis of the $H_{II\delta}$ phase in any significant way.) Off-specular reflection from vertical substrates recorded three peaks (−1,1), (1,0), and (1,1) of the $H_{II\delta}$ phase. Off-specular reflection from horizontal substrates recorded (−1,1), (1,0), (2,0), and (−2,2). The three peaks on q_z, (0,1), (0,2), and (0,3), were measured by oscillating ω scan.

Off-Specular Reflection. The intensities of the diffraction peaks were integrated directly on the detector image in two ways. (1) The peaks (including those of the coexisting hexagonal phase) were fit by two-dimensional Gaussian functions plus a background, and then integrated. (2) The peaks were first integrated

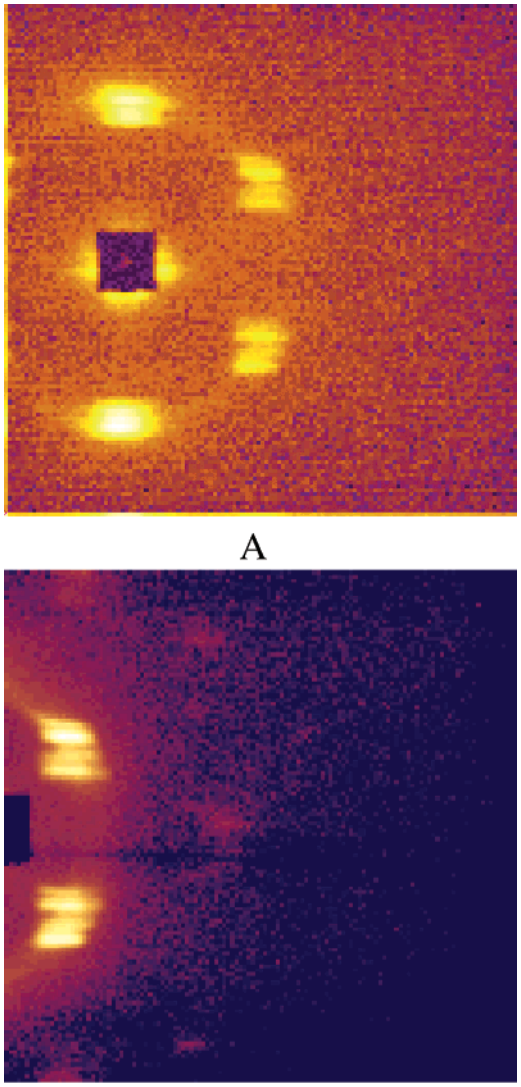

Figure 2. Reflection image produced by horizontal sample on the area detector. The sample substrates were held approximately horizontal. The exact orientation of the substrates was determined by the line shadow of the substrates (about 1° and slightly tilted). (A) The detector was 4.98° from the incident beam and the exposure time was 5 min. The peaks were smeared in the vertical direction due to the vertical beam divergence. (B) The detector was at 12° from the incident beam, and the exposure time was 7 h to detect possible higher orders in the high q_x region. The line shadow of the wafers is visible in this image. The peaks are identified by referring to Figure 4 (q_z is vertical). (0,1), (1,0), and (−1.1) are visible in (A). (1,1), (1,0), (−1,1), (2,0), and (−2,2) are visible in (B). The weak peak near the geometrical center of the detector in (B) belongs to the coexisting hexagonal phase.

(20) Yang, L.; Harroun, T. A.; Heller, W. T.; Weiss, T. M.; Huang, H. W. Neutron off-plane scattering of aligned membranes I. Method of measurement. *Biophys. J.* **1998**, *75*, 641−645.

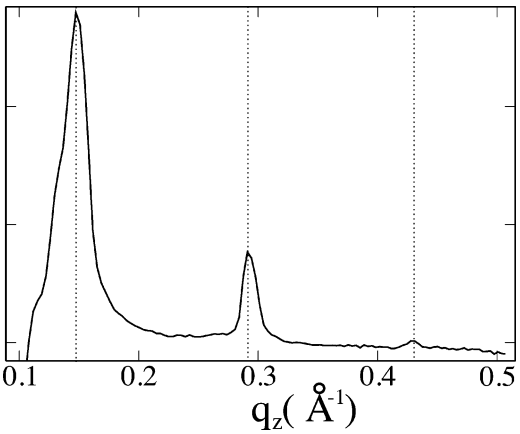

Figure 3. Oscillating ω scan: All the data at different ω were summed to obtain one diffraction pattern on the q_z. The shoulder of the first peak was due to the coexisting hexagonal phase (see Figure 1). The coexisting hexagonal peak was removed by fitting the first peak by two Gaussians with known positions from Figure 1.

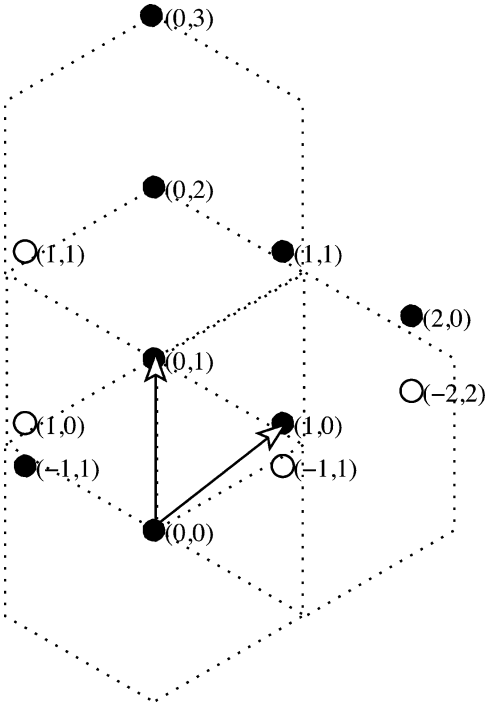

Figure 4. The distorted hexagonal (2D monoclinic) lattice. The basis vectors are $\mathbf{b_1}(q_x = 0.150 \sin 53°, q_z = 0.150 \cos 53°)$ and $\mathbf{b_2}(0,0.150)$ in the unit of Å^{-1}—q_z vertical, q_x horizontal. The small circles (both filled and unfilled) are the detected peaks. The filled circles are the lattice points of the basis vectors. The unfilled circles are produced by rotating the lattice around q_z by 180°.

in the q_x direction over a width slightly wider than the apparent peak widths. The result was plotted along the q_z axis. On this 1D profile, the background was obtained by using the intensities between the peaks and extrapolated into the peak regions. After the background removal, each peak was fit with a Gaussian and then integrated along the q_z direction. The results of the two methods were consistent with each other.

Oscillating ω Scan. All the data at different ω were summed to obtain one diffraction pattern along q_z (Figure 3). The peak intensities were integrated in the same manner as for the off-specular reflection.

The integrated peak intensities E of the $H_{II\delta}$ lattice were then reduced to obtain the magnitudes of the relative amplitudes F for the unit-cell form factor. The procedure for the reduction was described by Yang and Huang[14] and is recapitulated in Table 1. Note that reflections from both vertical and horizontal substrates covered the (1,0) and (−1,1) peaks. The reduced amplitudes for these two peaks were consistent between these two independent measurements.

Normalization between Off-Specular Reflection and Oscillating ω Scan. One normally obtains integrated peak intensities from a single crystal by collecting the diffraction intensity while rotating the sample[21] as in the oscillating ω scan. On the other hand one obtains integrated peak intensities directly from powder diffraction since the sample can be regarded as rotating without change. Here we have an unusual situation that one part of the diffraction pattern was obtained from an oscillating ω scan and another part of the pattern from an off-specular reflection that was an in-plane powder diffraction.

The relative normalization is given in the last row of Table 1. The ΔT for the off-specular reflection is the scan time. The Ω for the oscillating ω scan is the angular velocity given by the step size in radians divided by the scan time for each step. Thus the normalization factor for the oscillating ω scan is $2\pi/\Omega = \pi(0.125/180)/\Delta T$. This normalization procedure has been tested and proven to be correct in the hexagonal phase where the hexagonal symmetry demands that the amplitude measured by oscillating ω scan along the q_z axis must be the same as the amplitude measured by off-specular reflection off the q_z axis.[11]

Results and Discussion

Distorted Hexagonal Phase. The reciprocal vectors of the 2D monoclinic lattice are $\mathbf{b_1}(q_x = 0.150 \sin \gamma, q_z = 0.150 \cos \gamma)$ and $\mathbf{b_2}(0,0.150)$ at $\gamma = 53°$. This lattice is the same as that previously measured by X-ray diffraction on nondeuterated DOPC/DOPE 1:1 mixture ($|\mathbf{b_1}| = |\mathbf{b_2}| = 0.151$ Å^{-1} and $\gamma = 53.8°$) and identified as the $H_{II\delta}$ phase.[10] When the hydration level of the sample increased, the coexisting hexagonal peaks became weaker and disappeared, but simultaneously a weak coexisting rhombohedral phase would appear. It is possible that there is a small range of RH where the sample is in a pure $H_{II\delta}$ phase, but we did not have fine control of RH to fine-tune the sample condition.

It is apparent from the sample preparation that the sample consisted of domains (polycrystalline) with the x-component of $\mathbf{b_1}$ randomly oriented in the plane of the substrates. Thus in reciprocal space each lattice point was distributed in a circle parallel to the substrate and centered around the axis q_z. Each circle of the lattice points will be registered as a diffraction peak on the detector if the circle intercepts the Ewald sphere. The diffraction pattern on the detector is symmetric with respect to q_z, i.e., each lattice point appeared both on the right and on the left side of q_z. The detected peaks of the $H_{II\delta}$ phase are shown in Figure 4. The coexisting regular hexagonal peaks have been removed.

Phase Determination by D_2O/H_2O Exchange. This method of phase determination was recently demonstrated with an inverted hexagonal phase of diphytanoyl phosphatidylcholine (DPhPC) and was fully discussed by Ding et al.[11] The principle is simple. Express the diffraction amplitude of a lipid−water system as

$$A_H(\mathbf{q}) = \sum_{i \in L} b_i e^{\mathbf{iq}\cdot\mathbf{r}_i} + \sum_{j \in W} b_j^{H_2O} e^{\mathbf{iq}\cdot\mathbf{r}_j} \qquad (1)$$

where b_i stands for the coherent scattering amplitude or the scattering length of the ith element at position r_i. We have separated the sum over the elements to two parts,

(21) Warren, B. E. *X-ray Diffraction*; Dover: New York, 1969; pp 41−49.

Table 1. Formula for Data Reduction[a] (Yang and Huang, 2003, see Note below) $E = I_o|F|^2 C_p C_L C_{abs} C_{geo} \Delta T$

off-specular reflection	ω scan
$C_p = \sin^2 \psi$	$C_p = \cos^2 2\theta$
$C_L = 1/(\cos \alpha \cos \nu \sin \gamma)$	$C_L = 1/(\sin 2\theta)$
$C_{abs} = \{1 - \exp[-\mu a((1/\sin \nu) + (1/\sin \alpha))]\}/\{\mu a((1/\sin \nu) + (1/\sin \alpha))\}$	$C_{abs} = ([1 - \exp(-2\mu a/\sin \theta)] \sin \theta)/2\mu a$
$C_{geo} = (b/\sin \alpha)/w$ or 1 if greater than 1	$C_{geo} = (b/\sin \alpha)/w$ or 1 if greater than 1
ΔT	$2\pi/\Omega$

[a] Notations: ψ = the angle between the incident polarization vector and the scattered beam; α = the angle between the incident beam and the substrate surface (the $x - y$ plane); ν = the angle between the diffracted beam and the $x - y$ plane; γ = the angle between the in-plane $(x - y)$ projection of incident beam and the in-plane projection of the diffracted beam; μ = the linear absorption coefficient of sample; μ_s = the linear absorption coefficient of substrate; a = the sample thickness; a_s = the substrate thickness. The polarization factor C_p is for X-ray diffraction only. C_{abs} in the table is for reflection geometry. For transmission geometry the absorption correction is $C_{abs} = \exp[-(\mu_s a_s + \mu a)/(\sin \alpha)]\{1 - \exp[-\mu a((1/\sin \nu) - (1/\sin \alpha))]/[\mu a((1/\sin \nu) - (1/\sin \alpha))]\}$. C_{geo} is the ratio of the length of the beam footprint b/sinα over the length of the sample. ΔT is the scan time. Ω is the angular velocity of the ω-scan. Note: In comparison with the formulas given in Yang and Huang (2003), note the typos in the latter including the definitions for angles ν and γ, and expressions for C_{abs}. Also in Table 1 we have eliminated the redundant angles β and ω used in the reference.

for lipid (L) and for water (W). If part of the water is replaced by D_2O, the amplitude can be written as

$$A_{DH}(\mathbf{q}) = \sum_{i \in L} b_i e^{i\mathbf{q}\cdot\mathbf{r}_i} + \sum_{j \in W} [b_j^{H_2O} + x(b_j^{D_2O} - b_j^{H_2O})] e^{i\mathbf{q}\cdot\mathbf{r}_j} = A_H(\mathbf{q}) + xRA_{D_2O}(\mathbf{q}) \quad (2)$$

where x is the D_2O fraction of the D_2O/H_2O mixture, $R = (b_j^{D_2O} - b_j^{H_2O})/b_j^{D_2O}$ is a positive constant, and $A_{D_2O}(\mathbf{q})$ is the diffraction amplitude if only the water (replaced completely by D_2O) molecules in the lipid−water system contribute to the diffraction. Equation 2 has two applications.

(1) Experiment determines only the absolute magnitude of the amplitude. If a diffracting system is centrosymmetric, its diffraction amplitudes are real. In that case, the magnitude $|A_{DH}(\mathbf{q})|$ varies linearly with x. On the other hand, if the diffraction amplitudes are complex, the magnitude $|A_{DH}(\mathbf{q})|$ is in general not a linear function of x. Therefore a plot of the magnitude $|A_{DH}(\mathbf{q})|$ as a function of x provides a test for whether the system is centrosymmetric or not. (2) If the system is centrosymmetric, $A_{DH}(\mathbf{q})$, $A_H(\mathbf{q})$, and $A_{D_2O}(\mathbf{q})$ are all real and either positive or negative. Then there are three possible cases for the experimental values of $|A_{DH}(\mathbf{q})|$: either it linearly increases or decreases with x or it linearly decreases with x to zero and then linearly increases. Since $A_{D_2O}(\mathbf{q})$ determines the slope of $A_{DH}(\mathbf{q})$ as a function of x, in each case if the sign of $A_{D_2O}(\mathbf{q})$ is known, the sign of $A_{DH}(\mathbf{q})$ is determined. This method is most useful when it is possible to select a unit cell so that water is confined near the center, such as this case.

As shown in Figure 5, the magnitudes of the eight detected peaks are plotted against the variable x. Within the experimental errors, the linearity of $|A_{DH}(\mathbf{q})|$ as a function of x is satisfied. This implies that the lipid structure in the distorted hexagonal phase is centrosymmetric, which we believe is physically reasonable.

We know that in the inverted hexagonal phase water is at the center of the Wigner−Seitz cell. This must be also true in the distorted hexagonal phase. In fact the water molecules can be reasonably assumed to be in a Gaussian distribution centered at the origin of the unit cell. Hence all water amplitudes $A_{D_2O}(\mathbf{q})$ are positive. This implies that the signs of $A_{DH}(\mathbf{q})$ and $A_H(\mathbf{q})$ must be chosen so that $A_{DH}(\mathbf{q})$ has a positive slope as a function of x. With this method, the phases can be determined with confidence for at least six of the eight detected peaks as shown in Figure 5. The amplitudes for (2,0) and (−2,2) are very small, especially (−2,2), with considerable errors. Nevertheless the fact that they were clearly detectable at high values of x and not detectable at low values of x suggests the phases are positive so as to satisfy the condition of a positive slope. We will examine the other possible phase

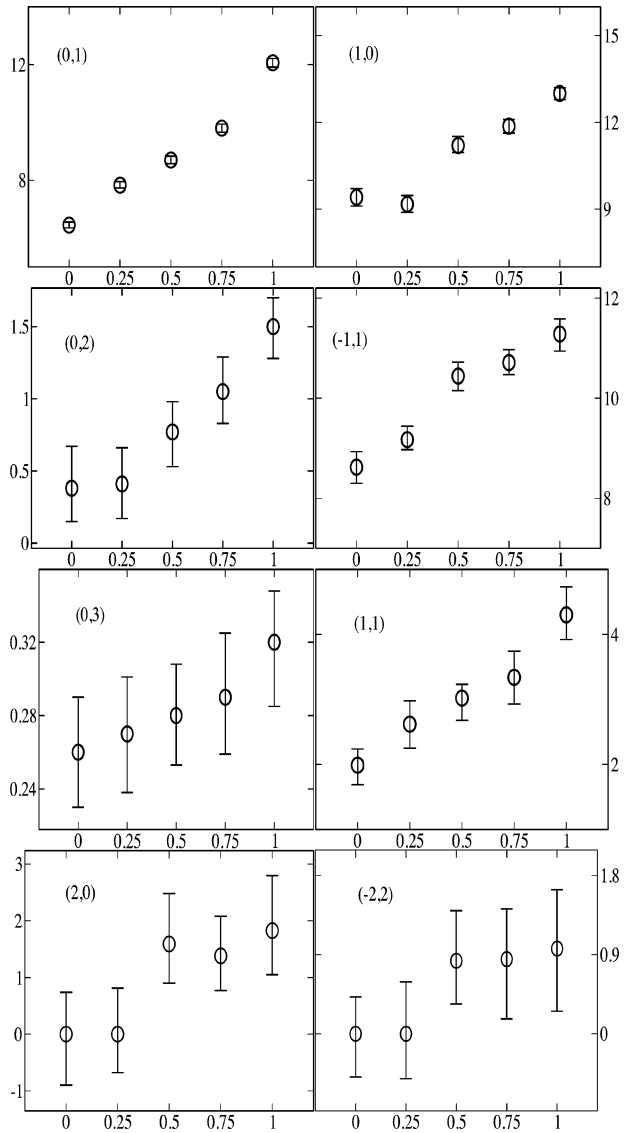

Figure 5. $A_{DH}(\mathbf{q})$ as a function of x. Ordinates: the diffraction amplitudes $A_{DH}(\mathbf{q})$ in all panels are in one arbitrarily chosen unit. Abscissas: x is the D_2O fraction of the D_2O/H_2O mixture used to hydrate the sample. The amplitude in each panel was plotted to have a positive slope. The largest source of error was from the uncertainties in the background removal; this was estimated for every peak individually. The statistical errors from the neutron counts are insignificant.

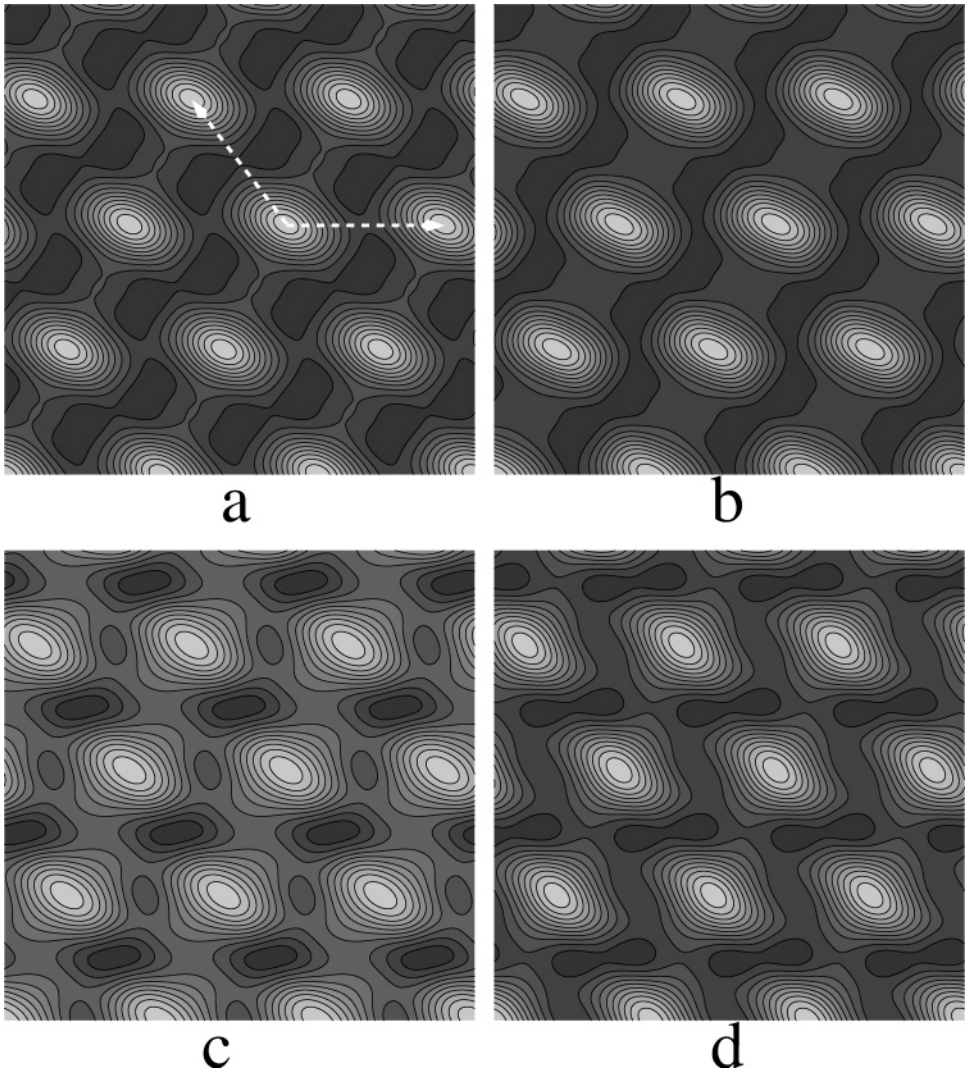

Figure 6. The neutron scattering length density distribution for 1:1 DOPC-d_{13}/DOPE hydrated by D_2O (high density is white, low density dark). The phase assignments for the first six peaks in Figure 5 are positive, and the phases for the (2,0) and (−2,2) peaks are (a) +,+; (b) +,−; (c) −,+; (d) −,−. The crystal vectors shown in (a) are $\mathbf{a_1}$(52.5 Å, 0 Å) and $\mathbf{a_2}$(−52.5 cos 53° Å, 52.5 sin 53° Å) in (a_x,a_z) with z vertical.

assignments for these two peaks to see if the results are physically reasonable.

The Structure of the Distorted Hexagonal Phase. The diffraction amplitudes with the chosen phases were used to construct the unnormalized neutron scattering length density in the unit cell

$$\rho(\boldsymbol{r}) = \sum_{H,K} A_{\mathrm{DH}}(\mathbf{q}_{H,K}) \cos(\mathbf{q}_{H,K}\cdot\mathbf{r}) \qquad (3)$$

where (H,K) denotes the lattice index (Figure 4). As determined above, the phases of all the peaks were chosen to be positive. For comparison we show other possibilities for the two weak peaks (2,0) and (−2,2). The results of neutron scattering length density distribution are shown in Figure 6.

It is important to note that the two reciprocal vectors $\mathbf{b_1}$ and $\mathbf{b_2}$ have the same magnitude. The corresponding crystal vectors $\mathbf{a_1}$(52.5 Å, 0 Å) and $\mathbf{a_2}$(−52.5 cos 53° Å, 52.5 sin 53° Å) also have the same magnitude. Therefore the line bisecting the angle between $\mathbf{a_1}$ and $\mathbf{a_2}$ is an axis of 2-fold symmetry for the lattice (so is the line bisecting $\mathbf{a_1}$ and $-\mathbf{a_2}$; see Figure 6A). It is reasonable to expect that the lipid structure within the unit cell satisfies this 2-fold symmetry as well. We see in Figure 6, the choice of the phases based on the D_2O/H_2O exchange, i.e., all phases positive, indeed gives a structure satisfying this 2-fold symmetry. On the contrary the phase assignments (−, +) and (−, −) for (2, 0) and (−2, 2) give a result that does not satisfy this symmetry. Although the result of the phase assignment (+, −) for (2, 0) and (−2, 2) is not very different from the (+, +) assignment, due to the smallness of the (−2, 2) peak, we believe that the all-positive phase assignment is the correct choice based on the argument of the D_2O/H_2O exchange.

Thus Figure 6a gives the neutron scattering length density distribution for the distorted hexagonal phase of DOPC-d_{13})/DOPE 1:1 mixture hydrated by D_2O at 56% RH. From eq 2, we obtained the diffraction amplitudes for the water and the lipid separately. In a previous study on diphytanoyl phosphatidylcholine, a model fitting found that at 58% RH there were about eight water molecules per lipid in the regular inverted hexagonal phase.[11] The neutron scattering length density distribution of the water (D_2O) in the $H_{II\delta}$ phase is shown in Figure 7a; the distribution for the lipid molecules is shown in Figure 7b on the same scale. Note that the center of the lipid structure did not show the expected low density. This is due to the coarse graining of low resolution. In a previous neutron diffraction study,[11] a regular inverted hexagonal

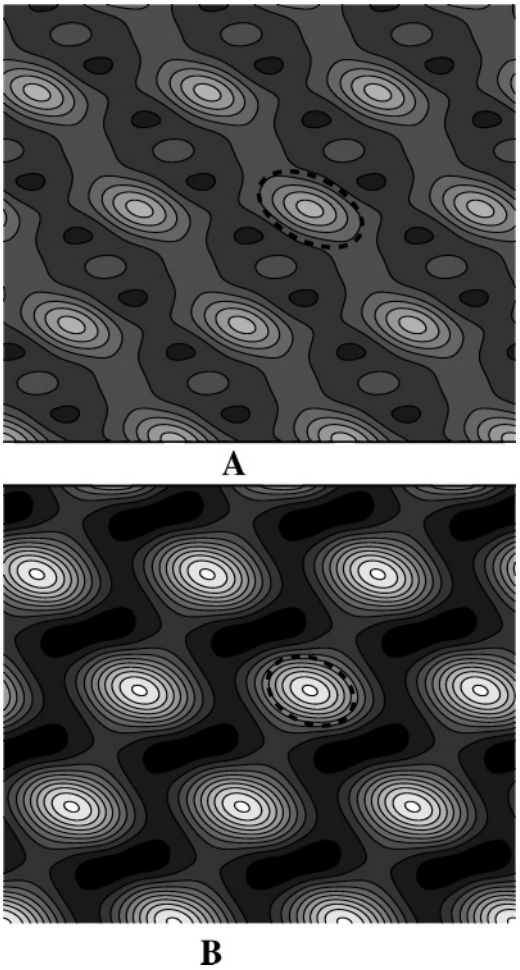

Figure 7. The neutron scattering length density distribution of (A) the water (D_2O) alone and (B) the lipid molecules (without water). The amplitudes of water and lipid are normalized to each other, and the density maps (A) and (B) are on the same scale. The dotted closed loops in A and B are each an equidensity contour whose closest distance from the center is 10 Å. Both contours are approximately elliptical. We use these reference contours to estimate the eccentricity of the density distribution.

phase diffracted to the fourth order (one higher than here) and its scattering length distribution showed an expected dip at the center of the lipid structure. However, if we artificially reduced its diffraction amplitudes by one order, the dip would disappear.

The equidensity contours of the distributions are oblong. The striking feature of Figure 7 is that the degree of elongation (or eccentricity) of water distribution is greater than that of the lipid distribution. We assume that along the minor axis of the roughly elliptical contours, the headgroup−chain interface is about 10 Å from the center, since the thickness of the headgroups is approximately 10 Å and the amount of water is small. The majority of the water molecules were very likely embedded among the headgroups.[22] We use this equidensity contour of 10 Å minor axis as a reference to measure the eccentricity of the roughly elliptical distributions (Figure 7). For the water distribution, the ratio of the major axis over the minor axis a/b of this reference contour is 1.75. For the lipid distribution, $a/b = 1.42$. On the basis of this experimental result, we will show that DOPC and DOPE

Table 2. Neutron Scattering Length Density (10^9 cm^{-2} or 10^{-7} Å^{-2})[a]

PC headgroup (phosphorylcholine-d_{13} + glycerol + carbonyl)	68
PE headgroup (phosphorylethanolamine + glycerol + carbonyl)	20
oleoyl chain	−2.2
CH_2	−2.9
CH_3	−8.3
H_2O	−5.6
D_2O	63.5

[a] The phospholipid component volumes were taken from Armen et al. (1998).

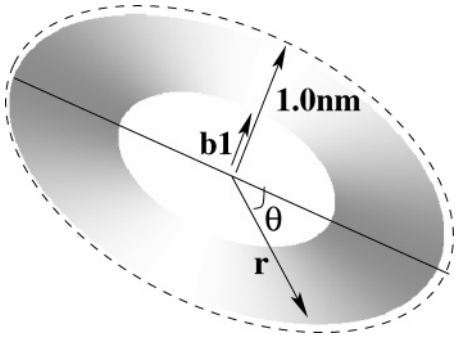

Figure 8. A model of POPE and DOPC distribution in a lipid tube of the $H_{II\delta}$ phase. An ellipse with a minor axis 10 Å and a ratio of the major axis over the minor axis $a/b = 1.75$ represents the interface between the headgroups and the chains. The gray scale implies a higher DOPE/DOPC ratio in the darker area. The density inside the small ellipse of minor axis b_1 and $a/b = 1.75$ is ρ_{max}. The density between the two ellipses is given by eq 4. A coarse graining factor $\exp[-(x^2 + y^2)/(\Delta)^2]$ is multiplied to each point.

are not distributed uniformly around the lipid tube in the $H_{II\delta}$ phase.

Nonuniform Distribution of DOPC and DOPE in the $H_{II}\delta$ Phase. Table 2 lists the neutron scattering length densities for parts of lipid molecules. It is clear that the most important contribution for the coherent neutron diffraction of lipid comes from the headgroups. The distinction between DOPC-d_{13} and DOPE is in the headgroup, not only the difference in deuteration but also the fact that PC is larger than PE in volume. DOPE has a larger spontaneous curvature (ca. −1/29 Å)[23] than DOPC (ca. −1/170 Å),[24] and the scattering length density is 20×10^9 cm^{-2} for PE, compared with 68×10^9 cm^{-2} for PC(d13).

It is reasonable to assume that the lipid interface closely follows the contour of the water distribution. We assume that the interface is approximately an ellipse of 10 Å minor axis and of $a/b = 1.75$ (Figure 8). If the lipid mixture packs uniformly around this interface, no matter the degree of coarse graining, it would not produce a scattering length density distribution with an $a/b = 1.42$ as in Figure 7B (see Figure 9a). Instead, we suppose a lipid distribution as depicted in Figure 8, with a higher concentration of DOPE near the vertexes where the curvature is the largest. To demonstrate that this can explain the difference between the eccentricities of water and lipid distributions, we consider a model Figure 8 that assumes a varying PE/PC distribution such that the weighted average of the scattering length densities of PE and PC is in proportion to the local curvature of the interface. The high density

(22) Hsieh, CH.; Sue, SC.; Lyu, PC.; Wu, WG. Membrane packing geometry of diphytanoyl phosphatidylcholine is highly sensitive to hydration: phospholipid polymorphism induced by molecular rearrangement in the headgroup region. *Biophys. J.* **1997**, *73*, 870−877.

(23) Leikin, S.; Kozlov, M. M.; Fuller, N. L.; Rand, R. P. Measured effects of diacylglycerol on structural and elastic properties of phospholipid membranes. *Biophys. J.* **1996**, *71*, 2623−2632.

(24) Szule, J. A.; Fuller, N. L.; Rand, R. P. The effects of acyl chain length and saturation of diacylglycerols and phosphatidylcholines on membrane monolayer curvature. *Biophys. J.* **2002**, *83*, 977−984.

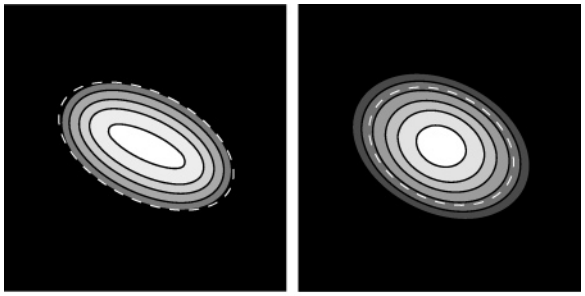

Figure 9. (a) The density distribution resulting from a uniform lipid distribution in the model shown in Figure 8. (b) The model equation (4) produced a distribution of contours similar to that of the lipid distribution shown in Figure 7B. The dotted closed loops in a and b are each an equidensity contour whose closest distance from the center is 10 Å.

at the center of the observed lipid density distribution, Figure 7B, is rationalized as follows. Because the PC headgroup is larger than the PE headgroup, and the three terminal methyl groups of PC are perdeuterated, the central region within the ellipse of minor axis b_1 (Figure 8) is most likely occupied by the deuterated parts of the cholines and, hence, assumed a scattering length density ρ_{max}. The scattering length density of the gray region between the interface and the inner ellipse is determined by the local PE/PC ratio as follows

$$\rho(\theta) = \rho_1 + \rho_2 K(\theta) = \rho_{min} + (\rho_{max} - \rho_{min})(K_{max} - K(\theta))/(K_{max} - K_{min}) \quad (4)$$

where K is the local curvature of the interface, i.e., that of the ellipse of 10 Å minor axis and $a/b = 1.75$: $K(\theta) = ab[a^2 \sin^2(\theta) + b^2 \cos^2(\theta)]^{-3/2}$. The magnitude of ρ_{min} was limited within the range $20 < \rho_{min} < 44$, i.e., below the average value of PC (68) and PE (20) and under the condition $\rho_{min} + \rho_{max} = 88$. The density at each point was then multiplied by a coarse-graining factor $\exp[-(x^2 + y^2)/(\Delta)^2]$. The coarse graining is caused by the thermal and static disorders in the sample as well as the instrumental resolution of neutron diffraction. The model with varying b_1, ρ_{min}, and Δ that produced a density distribution with $a/b \sim 1.42$ (Figure 9b) had $b_1 = 6$ Å, $\Delta = 6$ Å, and $\rho_{min} \sim 34$ ($\rho_{max} \sim 54$). The model implies that near the minor axis of the roughly elliptical lipid tube in the $H_{II\delta}$ phase the PE/PC ratio is about 2:5 whereas near the major axis the PE/PC ratio is about 5:2.

In principle, a more direct method for determining the distribution of deuterated PC is by measuring the difference between the present sample and a nondeuterated 1:1 DOPC/DOPE counterpart under the identical condition. However, in practice it is difficult to prepare two such samples to an identical condition. As mentioned in the Experimental Section, there are considerable uncertainties in the hydration condition of the sample due to the hysteretic nature of the hydration dependence and the lack of fine control of the humidity chamber. Furthermore, some changes in the phase diagram due to deuteration, as noted in the case of DPhPC,[11] cannot be ruled out. Nevertheless the original plan of this experiment included a comparison with a nondeuterated sample. It was not done due to the limitation of the neutron beamtime.

Conclusion and Remarks

Bending transitions of lipid bilayers, such as what happen during membrane fusion and in the formation of transmembrane pores, are very important, fascinating, and still not understood, although steady progress has been made.[25−27] The logical places to look for the mechanisms of bending transitions are the lipid phase transitions that involve a change of monolayer curvature. Indeed much about the lipid rearrangements during membrane fusion has been learned from the studies of the lamellar-inverted hexagonal transitions[3,4] and more recently of the lamellar-cubic transitions[28] as a function of temperature. The mechanism for both of these two transitions is the increase of lipid's spontaneous curvature with temperature, as pointed out by Gruner.[29] Here we show that another variable, i.e., dehydration, can induce a rich variety of bending transitions in a lipid mixture. Starting from the lamellar phase of a homogeneous DOPE/DOPC mixture in full hydration, dehydration causes local contacts between bilayers, that is followed by the subsequent merging of apposed monolayers at the contact points and the whole system stabilized in a rhombohedral lattice of stalk structures.[13,14] Further dehydration first transforms the stalk phase to a distorted inverted hexagonal phase, and then at lowest hydrations to a regular inverted hexagonal phase. In this paper, we used selected deuteration of lipid and water to solve the structure of the distorted hexagonal phase and showed evidence that the DOPE/DOPC ratio varied around the approximately elliptical lipid tube in the unit cell. Thus for the first time we show that demixing of lipid components can play a role in bending transitions. It is highly probable that the lipids are demixed in the stalk structure as well. From this sample the neutron diffraction of the rhombohedral phase was limited to only a few peaks; therefore it was not analyzed.

Single-component lipid, including DPhPC,[14] DOPE,[10] monomethylated DOPE and dimethylated DOPE (unpublished results) exhibited regular hexagonal phases, but not the distorted hexagonal phase. The fact that only lipid mixtures exhibit the distorted hexagonal phase suggests that a noncircular lipid tube requires a variable in the mixing ratio of the lipid components. The bending energy of a lipid tube is lowered if the local spontaneous curvature of the lipid mixture is adjustable according to the local curvature (this does not imply the equality of the local spontaneous curvature to the actual local curvature). This also implies that lowering the mechanical energy overcomes the free energy cost of demixing.

We make two points in conclusion. (1) Demixing of lipid components is a potential variable in the free energy of bending transitions. (2) In the search for the mechanisms by which proteins induce bending transitions of lipid bilayers, it is worthwhile to study both the dehydration-induced and temperature-induced lipid phase transitions.

Acknowledgment. We acknowledge the support of the Institut Laue-Langevin in providing the neutron research facilities used in this work. This work was supported by NIH Grants GM55203 and RR14812 and by the Robert A. Welch Foundation (to H.W.H.).

LA047876U

(25) Lentz, B. R.; Malinin, V.; Haque, M. E.; Evans, K. Protein machines and lipid assemblies: current views of cell membrane fusion. *Curr. Opin. Struct. Biol.* **2000**, *10*, 607−615.

(26) Lentz, B. R.; Siegel, D. P.; Malinin, V. Filling potholes on the path to fusion pores. *Biophys. J.* **2002**, *82*, 555−557.

(27) Huang, H. W.; Chen, F. Y.; Lee, M. T. Molecular mechanism of peptide-induced pores in membranes. *Phys. Rev. Lett.* **2004**, *92*, 1983042002.

(28) Siegel, D. P.; Kozlov, M. M. The Gaussian curvature elastic modulus of N-monomethylated dioleoyl phosphatidylethanolamine: relevance to membrane fusion and lipid phase behavior. *Biophys. J.* 2004, in press.

(29) Gruner, S. M. Stability of lyotropic phases with curved interfaces. *J. Phys. Chem.* **1989**, *93*, 7562−7570.